Tutor/s

Dr. Federico Calle Vallejo

UNIVERSITAT DE BARCELONA

Treball Final de Grau

Pt alloys with transition metals for hydrogen evolution

Lluís Ferrer Sarget

06/2022

Mai sabrem el valor de l'aigua fins que el pou estigui sec.

Thomas Fuller

En aquest racó m'agradaria deixar constància de la meva gratitud cap a totes aquelles persones, pertanyents a l'àmbit acadèmic i personal, que m'han ajudat a créixer professionalment i com a individu.

En primer lloc, voldria agrair a Federico, el meu tutor en aquest treball, per tots els coneixements que m'ha transferit i la paciència dipositada per fer-ho.

A continuació, agrair als meus pares, Romà i Núria, i a la meva germana Montse, tota la força que m'han donat per continuar endavant i no rendir-me a pesar de les dificultats.

Finalment, mostrar gratitud als meus companys de carrera, en especial a la Júlia, la Clara i el Christian, pel viatge acadèmic que hem viscut. Sense ells no hauria estat igual.

CONTENTS

SUMMARY

Nowadays, the use of fossil fuels is exaggerated and the development and optimization of technologies capable of fulfilling human society's energetic needs is utterly important. Not only fossil fuels are a non-renewable source of energy, but they are also harmful for the environment and the population. A possible alternative for replacing fossil fuels and internal combustion energies for automotive applications are low-temperature fuel cells. The fuel used in those cells is H_2 and the electrochemical process only produces water as by-product. Sustainable supply of H_2 must be guaranteed if those technologies are to be globally adopted. However, currently more than 90 % of the H_2 produced comes from steam reforming of natural gas and other light fossil fuels. Alternatively, hydrogen can be produced electrochemically by means of the hydrogen evolution reaction (HER) in water electrolyzers. The best catalyst for that purpose is platinum, an expensive and scarce metal. Therefore, alloying is an appealing option to reduce the loading of Pt during hydrogen evolution. Furthermore, positioning a subsurface layer of transition metals increases the activity of the electrolyzer. In this research work, using density functional theory calculations, the computational hydrogen electrode and a simple descriptor-based analysis, we determined the best near-surface alloys (NSAs) of Pt and transitions metals for the HER. We determined that for (111) facets of Pt NSAs the best alloying candidates are Fe, Co and Re. Instead, for (100) facets of Pt NSAs the best alloying candidates are Y and Mo.

Keywords: hydrogen evolution reaction, electrocatalysis, near-surface alloys, density functional theory, VASP, free energy of adsorption, volcano plot.

RESUM

Avui en dia, l'ús de combustibles fòssils és exagerat i el desenvolupament i optimització de tècniques capaces de satisfer les necessitats energètiques de la nostra societat és imprescindible. No només els combustibles fòssils són una font d'energia no renovable, sinó que també són perjudicials per al medi ambient i la població. Una possible alternativa per substituir els combustibles fòssils i les energies de combustió interna per a aplicacions d'automoció són les piles de combustible de baixa temperatura. El combustible utilitzat en aquestes piles és H_2 i el procés electroquímic només produeix aigua com a producte. Per adoptar aquestes tecnologies a nivell mundial s'ha de garantir el subministrament sostenible d'H_2. En aquest moment, però, més del 90% de l'H_2 produït prové del reformat de gas i altres combustibles fòssils més lleugers. Alternativament, l'hidrogen es pot produir electroquímicament per mitjà de la reacció d'evolució de l'hidrogen (HER). El millor catalitzador per a aquest propòsit és el platí, un metall car i escàs. Per tant, l'aliatge és una opció atractiva per reduir la quantitat de Pt per l'evolució de l'hidrogen. A més, posicionar una subcapa de determinats metalls de transició augmenta l'activitat de l'electròlit. En aquesta treball d'investigació, utilitzant càlculs de teoria de funcions de densitat, l'elèctrode computacional d'hidrogen i un anàlisi simple basat en un descriptor, determinarem els millors aliatges propers a la superfície (NSAs) de Pt i altres metalls de transició per a l'evolució d'hidrogen. En aquest treball es determina que, per a superfícies (111) de NSAs de Pt, els millors candidats d'aliatge son Fe, Co i Re. En canvi, per a superfícies (100) de NSAs de Pt els millors candidats son Y i Mo.

Paraules clau: reacció d'evolució de l'hidrogen, electrocatàlisi, aliatges propers a la superfície, teoria del funcional de la densitat, VASP, energia lliure d'adsorció, diagrama de volcà.

SUSTAINABLE DEVELOPMENT GOALS

The sustainable development goals are a set of global objectives for a better and more sustainable future. The goals are to end poverty, protect the planet and ensure that all people enjoy peace and prosperity now and in the future.

The present study focuses on increasing the activity of electrodes for the evolution of hydrogen and thus reducing the energy losses associated with their insufficient activity and their high prices. This research work aimed to determine appealing electrocatalysts for electrochemically producing hydrogen, such that hydrogen-based technologies spread worldwide and become an alternative fuel source to fossil fuels and internal combustion energies. At the same time, we intended to reduce the amount of platinum used for the electrodes by alloying it with other transition metals.

For these reasons, our research is of great interest and it can have a great impact in two of the major areas that guarantee sustainable development. These two areas are:

- Prosperity Area
- Planet Area

Finally, the sustainable development goals which the project is related with are listed below, together with the targets and indicators where the research can be included in the 2030 Agenda for sustainable development:

Goal 7: Clean and affordable energy.

Target 7.1: Ensure universal access to affordable, reliable and modern energy services.

Indicator 7.1.2: Proportion of population with primary reliance on clean fuels and technology.

Goal 8: Decent work and economic growth.

Target 8.2: Achieve higher levels of economic productivity through diversification, technological upgrading and innovation.

Target 8.4: Improve progressively global resource efficiency in consumption and production and try to separate economic growth from environmental degradation.

Goal 9: Industry, innovation and infrastructure.

Target 9.4: Adapt industries to make them sustainable, with increased resource-use efficiency and greater adoption of clean and environmentally sound technologies and industrial processes.

Indicator 9.4.1: CO_2 emission per unit of value added.

Goal 11: Sustainable cities and communities.

Target 11.2: Safe, affordable and sustainable transport Systems.

Indicator 11.2.1: Proportion of population that has convenient access to public transport, by sex, age and persons with disabilities.

Goal 12: Responsible consumption and production.

Target 12.2: Achieve the sustainable management and efficient use of natural resources.

Indicator 12.2.1: Material footprint, material footprint per capita, and material footprint per GDP.

Target 12.8: Ensure that people everywhere have the relevant information and awareness for sustainable development and lifestyles in harmony with nature.

Indicator 12.8.1: Extent to which education for sustainable development is mainstreamed.

Target 12.a: Support the movement towards more sustainable patterns.

Indicator 12.a.1: renewable energy-generating capacity.

Goal 13: Climate action.

Target 13.2: Integrate climate change measures.

Indicator 13.2.2: Total greenhouse emissions per year.

1. INTRODUCTION

The main motivation of this project is the optimization of the electrodes used to produce hydrogen. Those electrodes are made up of platinum. The question remains as to why alloying platinum with other metals for hydrogen production is advisable. In short, there are two main reasons: the first reason lies in the reduction of the amount of platinum needed to manufacture the electrodes. Alloying Pt with a less expensive and more abundant element most likely lowers the overall cost of water electrolyzers. The second reason is the increase in activity provided by the alloying metal, specifically by positioning a subsurface layer of a certain transition metal. Greater activity results ultimately in energy savings.

Simulations can be made using programs based on density functional theory to determine the adsorption free energies of hydrogen. As those energies are linked to the respective hydrogen evolution activities, in principle, it is possible to determine the most promising alloys by analysing the adsorption energies. Specifically, this work focused on obtaining the free energies of adsorption of hydrogen using the VASP program and, together with a theoretical background based on thermodynamics and descriptor-based analysis, we determined the most promising near-surface alloys of Pt and transition metals.

2. OBJECTIVES

The main objective of this project is to determine the most active Pt NSAs for hydrogen evolution.

In order to accomplish the main objective, we set the following specific tasks:

- Familiarization with DFT calculations and hydrogen evolution.
- Learning how to work in the Linux environment.
- Learning how to perform DFT calculations with VASP.
- Simulation of the adsorption of hydrogen on NSAs with VASP.
- Assessment of the free energies of adsorption of hydrogen.
- Prediction of the activities via a volcano plot.

3. BACKGROUND

3.1. HYDROGEN REACTION EVOLUTION

Hydrogen (H2) can be produced from water by virtue of heterogeneous redox reactions at electrified interfaces in a device called water "electrolyzer". The electrolyzer has a global reaction ($2H_2O \rightarrow 2H_2 + O_2$) in which water is split and two half reactions: the cathodic hydrogen evolution reaction (HER, $4H^+ + 4e^- \rightarrow 2H_{2(g)}$) and the anodic oxygen evolution reaction (OER, $2H_2O \rightarrow O_2 + 4H^+ + 4e^-$). Both the HER and the OER can be improved via catalyst optimization. The state-of-the-art catalyst for the HER is platinum, which is an expensive and scarce material. The amount of platinum needed for modern polymer electrolyte membrane (PEM) electrolyzers can be reduced by selectively positioning a monolayer of copper in the electrode (Tymoczko et al., 2016). A brief explanation to this is that copper in the subsurface layer of platinum lowers the surface binding of adsorbed hydrogen intermediates (*H), which is convenient because Pt sits on the strong-binding side of the HER volcano plot, see Figure 1.

Currently, approximately only 4 % of H_2 currently comes from water electrolysis (Bicakova & Straka, 2012). The main barrier to introduce this technology as the main approach to obtain hydrogen are the energy losses associated to the insufficient activity of electrodes. The material expenses are relatively small compared with the additional costs linked to the extra electricity to be supplied in view of the lack of activity of the catalysts.

3.1.1. General considerations

According to the Sabatier principle, the optimal catalytic surface should bind reaction intermediates moderately. For the HER, the intermediate is adsorbed hydrogen, denoted *H. Quantitatively, this statement can be rationalized using calculated or measured adsorption energies and comparing them for different pure metal surfaces. Figure 1, which is known as a Sabatier-type volcano plot, shows that the optimum material for the electrocatalytic HER displays binding energies slightly weaker than Pd, Rh or Pt.

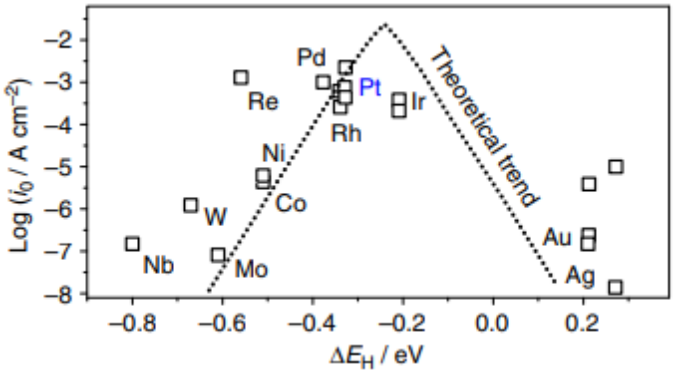

Figure 1. Experimental HER activity expressed as the exchange current density, log(i0), for different metal surfaces as a function of the calculated *H chemisorption energy, ΔEH. Taken from (Tymoczko et al., 2016).

The binding energy (ΔEH) displayed in Figure 1 was estimated via density functional theory (DFT) calculations. DFT is a computational quantum mechanical modelling method used to investigate the electronic structure of atoms, molecules and condensed phases. The binding energy depends on the composition and coordination of the surface site where *H is adsorbed (Tymoczko et al., 2016) (Pohl et al., 2017). The possible hydrogen locations on the (111) facet and on the (100) facet are shown Figure 2.

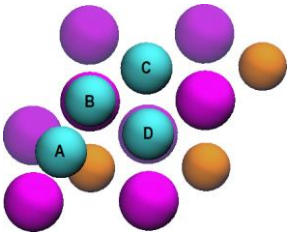

(**a**)

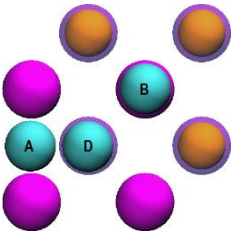

(**b**)

Figure 2. Possible adsorption sites for *H. (a) (111) facet of an fcc metal. (b) (100) facet. A) bridge, B) top, C) FCC hollow and D) HCP hollow. Purple atom: Pt, blue atom: H, orange atom: Cu in the subsurface.

The electronic properties of a pure metal electrode can be modified by means of different approaches. Bulk alloys are an excellent option, where every atomic layer (except perhaps for the surface layer) has the same composition. In addition, one can also resort to positioning atomic layers of solute metals to form overlayers, surface or subsurface alloys.

3.1.2. Electrochemical performance

The effect of modifying the electronic properties can be seen in the cyclic voltammograms (CVs) in Figure 3, which were recorded in Ar-saturated 0.1 M HClO4 electrolyte. Cyclic voltammetry is an electrochemical technique that measures the resulting flow of electrons upon changing the potential of a working electrode in a cyclic manner between a lower and upper value, at a certain speed in mV/s. The experiments in Figure 3 were performed for Pt(111), a Cu overlayer on top of Pt(111), a Cu-Pt (111) near-surface alloy (NSA) and a Cu-Pt surface alloy (SA). In the anodic sweep the potential is increased and the currents are positive. Instead, in the cathodic sweep the potential decreases and the current is negative. In the cathodic scan, the potential region between approximately 0.4 and 0.07 V refers to *H adsorption before the production of hydrogen. At more negative potentials H_2(g) is produced. Noticeably, the Cu-Pt SA (dotted blue line), approximately between 0.2 and 0.4 V, binds *H stronger than Pt(111) (solid black line) as the H-adsorption occurs at more positive potentials. In contrast, the Cu-Pt NSA structure (solid red line) weakens the binding compared to Pt(111) and an overlayer of Cu on top of Pt(111) (dashed orange line) does not seem to adsorb hydrogen at the potentials studied. The explanation for the noticeable changes in binding energies are the so-called “ligand effects”, due to Cu and Pt having different valence configurations.

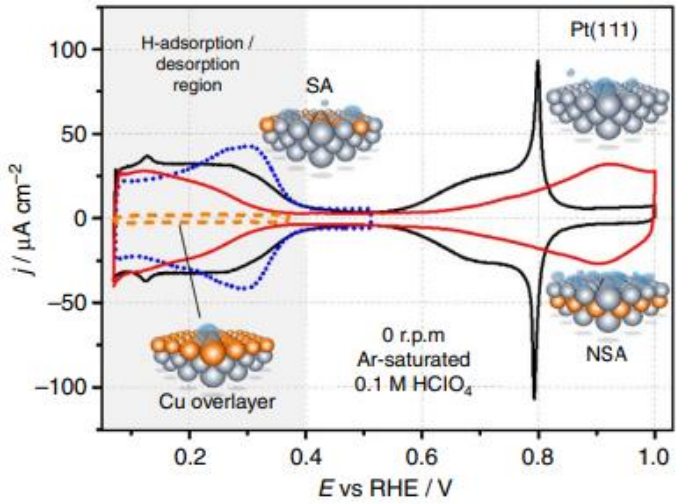

Figure 3. Cyclic voltammetry in Ar-saturated 0.1 M HClO4 recorded for Pt electrodes with different relative positions of the Cu atomic layer. SA: surface alloy. NSA: near-surface alloy. Taken from (Tymoczko et al., 2016). Sweeping speed: 50 mV/s.

Judging by the CVs in Figure 3, the location of the Cu-Pt SA should be on the left part of the volcano plot, at more negative binding energies than the top of the volcano and also more negative than Pt(111). For this reason, as the SA binds *H more strongly than Pt(111), it is less active for the HER. On the contrary, a Cu overlayer binds *H species too weakly and the HER does not occur. Finally, the Cu-Pt NSA surface binds *H slightly more weakly than Pt(111), such that it should be close to the theoretical maximum of the volcano plot. Figure 4 shows that the HER activities follow these predictions. Indeed, the Cu overlayer does not show any appreciable HER activity, the Cu-Pt SA is less active than platinum (111) and the Cu-Pt NSA reveals a higher activity towards HER than Pt(111).

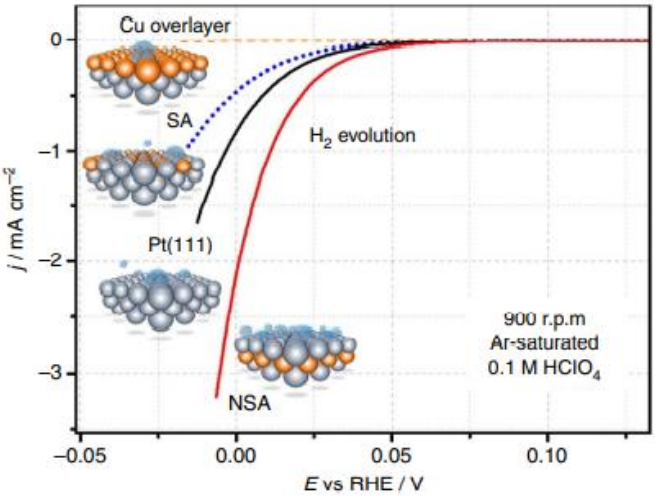

Figure 4. Rotating disk electrode (RDE) voltammetry at 900 rpm in Ar-saturated 0,1 M HClO4 for Cu overlayer, Pt(111), SA and NSA. Taken from (Tymoczko et al., 2016). Sweeping speed: 10 mV/s.

3.1.3. Computational

The experimental results are rationalized by means of computational results presented in Figure 5. First of all, Figure 5a presents the trends in *H adsorption for Pt(111), Cu-Pt NSAs and SAs. Noticeably, submonolayer amounts of Cu in the subsurface layer, at all concentrations, weaken the binding energies of hydrogen. Conversely, Cu on the top layer has the opposite effect, as justified previously. As more Cu is introduced the trends become more visible.

To address the fact that binding energies also change depending on the coordination of the adsorption sites (Tymoczko et al., 2016) (Pohl et al., 2017), various sites have to be tested, apart from the hollow sites at (111) terraces. Figure 5b gives information about the different adsorption energies for numerous sites at platinum (111) and NSAs with 1 ML of Cu in the subsurface. The results are provided as a function of the generalized coordination numbers $\overline{CN}$ of the surface sites. Briefly, generalized coordination numbers are a weight average in which each nearest neighbour is multiplied by its respective coordination number. This is equivalent to incorporating the second-nearest neighbours into the count (Pohl et al., 2017).

According to Figure 5b, sites with coordination lower than Pt(111) bind *H strongly, while sites with larger coordination the binding is weaker. Another important observation is that adsorption at NSAs is consistently weaker than on the same sites at unmodified Pt(111) by ~0.1 eV.

Moreover, Figure 5c displays the HER volcano-type activity plot. The figure reflects both the effect of coordination and Cu content on the HER activity. Defects with high coordination on pure platinum are considerably more active than Pt(111). This explains why polycrystalline platinum is more active than Pt(111) for the HER. Second, undercoordinated defects are less active than (111) terraces. On the other hand, both overcoordinated and undercoordinated sites on Cu-Pt NSAs bind H* less optimally than (111) Cu-Pt NSAs. This explains why (111) NSAs are more active than polycrystalline NSAs in experiments. Finally, SAs have no activity due to their strong adsorption energies.

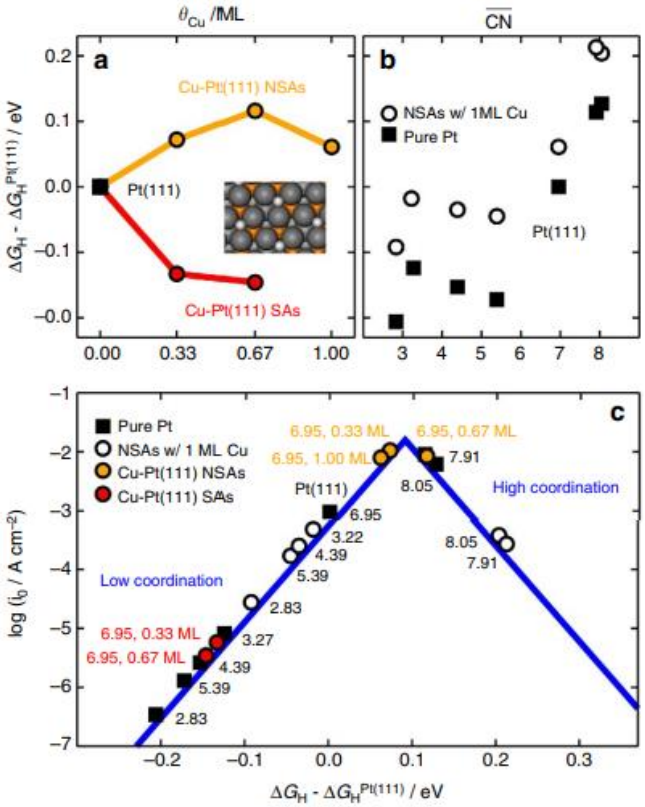

Figure 5. Computational trends in H_2 adsorption and evolution. (a) *H adsorption energies with surface Cu (SAs in red) and subsurface Cu (NSAs in orange) on Pt(111). The inset shows *H at a NSA with 0.67 ML Cu. (b) Adsorption energies of *H on Pt (black squares) and NSAs with 1 ML Cu (open circles) as a function of the generalized coordination numbers of the active sites. (c) Volcano plot showing the HER activity, coordination and composition of all studied sites. Taken from (Tymoczko et al., 2016).

3.2. **DFT** (ROGL ET AL., 2014)

Advanced computational approaches to predict material properties are based on density functional theory (DFT) and other methods. These first-principles calculations are able to calculate material properties at atomic and electronic levels and are based on quantum mechanics, classical mechanics, thermodynamics and electrodynamics. The rapid advance of computers has provided a strong driving force for computational materials science.

Quantum physical simulations are possible because not only computational power has increased a lot, but also in view of the enormous progress made in the development of computational algorithms. First-principles methods solve the Schrödinger equation that describes the interaction between electrons and nuclei. Approximations have to be made as no viable analytical solution can be found for a realistic system of interacting atoms. These approximations are improved using post DFT approaches.

First-principles calculations are free from empirical information and basic thermodynamic properties such as heat of formation can be calculated. In comparison to experimental procedures, DFT calculations are faster and many possible structures and compositions can be tested, which helps finding the true thermodynamic ground state. Forces on atoms and stresses can also be derived with the use of DFT electronic-structure calculations. This information is needed for optimizing structural parameters and for deriving vibrational properties. In addition, phonon calculations expand the applications for DFT calculations as temperature effects on the free energy can be added. A phonon is an excited state in the quantum mechanical quantization of vibrations for elastic structures of interacting particles.

3.3. **VASP** (*The VASP Manual - Vaspwiki*, n.d.)

Ab initio calculations can be done with the use of The Vienna Ab initio Simulation Package, also known as VASP. First, ab initio quantum chemistry methods are computational chemistry methods based on quantum mechanics, which is a branch of physics focused on describing the physical properties of nature at the scale of atoms and subatomic particles. Ab initio means “from first principles” or “from the beginning”. This means that the calculations are based on theory and not on experimentation.

Basically, the method used in this work to obtain the electronic energies is density functional theory (DFT), and additional corrections were performed to approximate the free energies of adsorption.

3.3.1. Inputs

In order to perform DFT calculations, VASP requires a number of inputs that have to be formulated with a correct syntax so that they can be correctly interpreted by the program. These inputs are:

POSCAR

This file contains the geometric data of all the atoms that are present in our study. The format of the POSCAR for a 2×2 (111) NSA of Pt and transition metals is:

```
Pt NSAs with transition metal elements
1.0
5.62352      0.00000 0.00000
2.81176      4.87011 0.00000
0.00000      0.00000 25.00000
Pt Sc H
12 4 1
Selective dynamics
Cartesian
0.00000 0.00000 0.00000    T T T      #first layer, Pt
2.81176 0.00000 0.00000    T T T
1.40588 2.43506 0.00000    T T T
4.21764 2.43506 0.00000    T T T
0.00000 1.62337 -4.59159   F F F      #third layer, Pt
2.81176 1.62337 -4.59159   F F F
1.40588 4.05843 -4.59159   F F F
4.21764 4.05843 -4.59159   F F F
0.00000 0.00000 -6.88738   F F F      #fourth layer, Pt
2.81176 0.00000 -6.88738   F F F
```

1.40588 2.43506 -6.88738 F F F

4.21764 2.43506 -6.88738 F F F

1.40588 0.81169 -2.29579 T T T #second layer, transition metal

4.21764 0.81169 -2.29579 T T T

2.81176 3.24674 -2.29579 T T T

5.62352 3.24674 -2.29579 T T T

0.014 0.009 1.811 T T T #ADSORBATE

The meaning of the lines present in the POSCAR file is:

- The first one is a comment line where, e.g., the name of the system is introduced.
- The second line provides a universal scaling factor used to scale all lattice vectors and all atomic coordinates. The value used in our research is 1.
- Lines 3-5 are reserved for the three lattice vectors that define the unit cell of our system.
- The sixth line gives information on the elements present in our system. For example, Pt, Sc and H for a NSA of Pt and Sc with H adsorbed on it.
- The seventh line lists the number of atoms present for each species in the same order as in the sixth line. In our example, there are 12 Pt atoms, 4 Sc atoms and one H atom.
- The eighth line must always remain the same and activates a mode to mark whether the coordinates of each atom can be modified or not during ion relaxation. This mode is called selective dynamics.
- The ninth line specifies how the atomic positions are provided. In this study the coordinates are given as Cartesian coordinates. Normally, the VASP output is given in direct coordinates.
- The next lines contain the three coordinates for each atom. Each line is dedicated for one atom and the order followed is the same as inserted in the sixth line of the POSCAR. The degrees of freedom for each atom and coordinate are to be supplied. T and F stand for true (relaxed) and false (fixed).

If no initial velocities are supplied the file ends here and has the necessary information for the program to be correctly executed.

POTCAR

This file has the pseudopotentials or projector augmented-wave method data. These data specify how many electrons are in the core of the atom and how many are in the outer shell and how to approximate the interactions between the core and the valence shell. The POTCAR contains information for each species involved in the calculation. It does not require the user to introduce or modify anything.

KPOINTS

This file specifies the Bloch vectors (k points) used to sample the Brillouin zone. The Brillouin zone is a uniquely defined primitive cell, repeating unit formed by the vectors spanning the points of a lattice, in reciprocal space. The number of k-points required depends on the system under study: large cells have small k-point samplings, whereas small cells have large k-point samplings. The KPOINTS file used in this research project has the following format:

automatically generated Monkhorst-Pack mesh

0

Monkhorst-Pack

6 6 1

0 0 0

The meaning of the lines present in the KPOINTS file is:

- The first line is a comment line. A Monkhorst-Pack grid is an unbiased method of choosing a set of points for sampling the Brillouin zone (Monkhorst & Pack, 1976).
- The second line specifies how the k points are set. It is 0 to indicate an automatic mesh generation.
- The third line determines the centre of the mesh. In this case, we have a Monkhorst-Pack scheme.
- In the fourth line the desired number of subdivisions are specified. In this case, the k-point sampling is 6×6×1. This sampling, together with the vacuum layer in the third vector of the POSCAR are suitable for the simulation of a surface.
- The fifth line is optional and allows the mesh to move slightly with respect to the default.

INCAR

This file determines what kind of calculation is to be carried out and how to do it. The algorithms and parameters that VASP uses during calculations are set and specified using INCAR tags. There are parameters for the electronic and ionic loops. The format of each statement consists of the name of the tag, the equal sign (=), and the value assigned to this specific tag, which can be a number or a string.

The INCAR file to calculate the DFT energies in this research project is the following:

SYSTEM = Pt alloy

PREC = Normal

ICHARG = 2

ISPIN = 1

ENCUT = 450.00

NELMIN = 6

ISMEAR = 2

SIGMA = 0.2

IBRION = 2

NSW = 500

POTIM = 0.25

EDIFF = 0.00001

EDIFFG = -0.01

NPAR = 4

LWAVE = F

LCHARG = F

The algorithms and parameters that these tags set are:

- SYSTEM: Helps the user define the use of the present calculation.

- PREC: Specifies the precision mode selected. PREC = Normal is used for most routine calculations. This parameter sets the defaults for four sets of parameters. This parameter sets the ENCUT parameter, but it is recommended to enter it manually to avoid incompatibilities between calculations.
- ICHARG: Determines how VASP constructs the initial charge density. Charge density is the amount of electric charge per unit of length, surface area or volume.
- ISPIN: Specifies whether the calculation is spin restricted or unrestricted. Spin-unrestricted calculations are to be performed for systems with unpaired electrons. ISPIN = 1 means spin-restricted calculations are made.
- ENCUT: The solution of the Kohn-Sham equations is to be expanded using a basis set. For systems with periodic boundary conditions, plane waves are ideal basis sets, and the accuracy of the basis set is given by the maximum energy of the plane waves. ENCUT specifies the cutoff energy for the plane-wave basis set in eV. It is an optional parameter as PREC sets the default parameter for ENCUT.
- NELMIN: Defines the minimum number of electronic self-consistency steps.
- ISMEAR: Determines how the partial occupancies are set for each orbital. For relaxations in metals ISMEAR = 2 (second order Methfessel-Paxton approach (Methfessel & Paxton, 1989)), for gases ISMEAR = 0 (Gaussian smearing).
- SIGMA: Establishes the width of the smearing in eV. For metals a reasonable value is SIGMA = 0.2. For molecules SIGMA = 0.001 is appropriate.
- IBRION: Determines how the ions are updated and moved. For difficult relaxation problems it is recommended to use IBRION = 2, namely, the conjugate gradient algorithm. IBRION = 2 possesses the most reliable backup routines and is used to relax the ions into their instantaneous ground-state. IBRION = 5 is used to carry out vibrational frequency analyses, see below.
- NSW: Sets the maximum number of ionic steps for the convergence of the structure.
- POTIM: For IBRION = 2, POTIM predetermines the step width of the ionic relaxation.
- EDIFF: Determines the global break condition for the electronic SC-loop. SC stands for self-consistent: the electronic density is calculated iteratively until there is negligible change in the results, in other words until the electronic density is “self-

consistent". This parameter is specified in units of eV. The relaxation stops when the free energy change and the band-structure-energy change between two steps are both lower than EDIFF.

- EDIFFG: Defines the break condition for the ionic relaxation loop. When this parameter is given a negative value, the relaxation is stopped when the norms of all the forces (in eV/Å) are smaller than $|EDIFFG|$. When positive it establishes the minimum energy difference between consecutive steps for which the calculation is deemed converged.
- NPAR: Defines the number of bands that are treated in parallel.
- LWAVE: Determines if the wavefunctions are written to the WAVECAR file at the end of a run. The WAVECAR usually provides excellent starting wavefunctions for restarting an unfinished job. Its writing can be avoided by setting LWAVE = F.
- LCHARGE: Determines if the charge densities are written and can also be used for restarting calculations. Similar to LWAVE, its writing can be avoided by setting LCHARGE = F.

The INCAR necessary to evaluate the vibrational frequencies and with those calculate the zero-point energy (ZPE) is, for the specific case of a hydrogen molecule:

SYSTEM = H2 molecule

PREC = Normal

ICHARG = 2

ISPIN = 1

ENCUT = 450.00

NELMIN = 6

ISMEAR = 0

SIGMA = 0.001

IBRION = 5

NFREE = 2

NSW = 480

POTIM = 0.02

ISYM = -1

EDIFF = 0.00001

EDIFFG = -0.01

NPAR = 4

LWAVE = F

LCHARG = F

All tags that have been added or modified to this INCAR file, in comparison to the previous one, appear above in bold. The modifications are:

- ISMEAR = 0: Gaussian smearing, normally used for molecules.
- SIGMA = 0.001: when ISMEAR = 0 is used, values of SIGMA close to zero are used.
- IBRION = 5: Allows the determination of the Hessian matrix (matrix of the second derivates of the energy with respect to the atomic positions) and the vibrational frequencies of the system.
- POTIM = 0.02: For IBRION = 5, POTIM is the width of the displacement of each ion to calculate the Hessian Matrix. Such displacements are to be small.

The additions are:

- NFREE: Number of displacements in each direction (x, y, z).
- ISYM: This parameter determines how VASP deals with symmetry. ISYM = -1 switches the use of symmetry completely.

3.3.2. Outputs

Once the calculation is finished, VASP gives several different output files. The most important output files are:

OUTCAR

This file gives detailed output of a VASP run including:

- Summary of the input parameters.
- Information of the electronic steps.

- Stress tensors.
- Forces on the atoms.
- Local charges and magnetic moments.
- Dielectric properties.
- Vibrational frequencies when IBRION = 5 is used.
- Total energies.
- Errors, if any.

OSZICAR

The OSZICAR file gives a short summary of the results:

- Chosen SC algorithm.
- Convergence of the total energy, charge- and spin densities.
- Total energies.
- Magnetic moments of the cell.

CONTCAR

This file is similar to a POSCAR file and gives the geometry data at the end of a run:

- Lattice parameters.
- Ionic positions in direct coordinates.
- The format of the CONTCAR is the same as the POSCAR and, in fact, the CONTCAR can be used to restart an unfinished calculation.

XDATCAR

This file contains updated ionic positions of each ionic step.

WAVECAR

This file contains the wave function coefficients and can be used to restart a calculation from a previous run.

3.4. **ADSORPTION ENERGY OF HYDROGEN AND HER OVERPOTENTIALS**

3.4.1. Thermodynamic theory of electrocatalytic reactions with two-electron transfers and one intermediate (HER)

Currently, the approaches for finding the best catalyst are primarily dictated by the thermodynamics of binding of the catalytic intermediates, as will be shown later in this work. There are different bottlenecks when catalysing the transfer of 1 and 2, or more than two electrons. Predictions about the optimal catalyst for these different reactions are made with thermodynamic considerations and with the use of DFT calculations. These concepts can be applied to the two-electron hydrogen oxidation and hydrogen evolution reaction.

The activation energy required to transfer two electrons is four times bigger than that of one single electron transfer. Thus, consecutive storage of charge in an intermediate is energetically more favourable. The overall rate is highly influenced by the interaction between the intermediate and the catalyst. The hydrogen evolution reaction (HER) is a two-electron transfer reaction with one intermediate:

$$2H^+ + 2e^- \leftrightarrows H_2 \quad (1)$$

The reaction has an equilibrium potential $E^0_{H2/H+}$ of 0 V. The standard hydrogen electrode (SHE) potential is declared at zero volts at any temperature. Three elementary steps are needed to describe the generally accepted mechanism of the HER on metals surfaces (Koper, 2011):

$$H^+ + * + e^- \leftrightarrows * \mathrm{H} \quad (1a)$$

$$* \mathrm{H} + H^+ + e^- \leftrightarrows H_2 + * \quad (1b)$$

$$2 * H \leftrightarrows H_2 + 2 * \quad (1c)$$

The steps are called, in order of appearance, the Volmer, Heyrovsky, and Tafel steps. The asterisk (*) represents an empty adsorption site on the metal electrode surface. *H is the species adsorbed on the electrode.

The mechanism shown previously includes two possible pathways. The Volmer step is always the first step to occur followed by either the Tafel or Heyrovsky step. In the Volmer/Tafel mechanism both hydrogens are adsorbed on the surface and in Volmer/Heyrovsky pathway only

one hydrogen is needed to adsorb. In Figure 6 a schematic representation of the two possible pathways is shown:

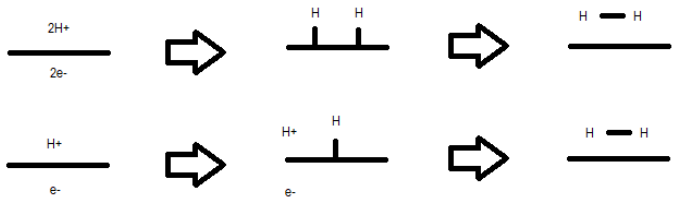

Figure 6. Possible pathways for HER mechanism. Volmer/Tafel (top) & Volmer/Heyrovsky (bottom).

The mechanism presented in Equations 1a-c has to fulfill thermodynamic constraints related to the combined equilibrium constants that need to conform to the Nernst equation of the global reaction. In case the reaction adopts the Volmer/Heyrovsky mechanism (Koper, 2011):

$$\frac{E^0{}_{H^+/*H} + E^0{}_{*H,H^+/H_2}}{2} = E^0{}_{H^+/H_2} = 0 \quad (2)$$

E^0, the standard equilibrium potential (or standard electrode potential), is defined as the equilibrium potential of an electrode reaction when all components are in their standard states, measured against the SHE. It describes the equilibrium between two different oxidation states of the same element. At equilibrium, the chemical driving force for an electrochemical reaction, ΔG is directly proportional to the electrical driving force, E in equilibrium. Considering the Volmer reaction (1a) with the equilibrium condition that follows (Koper, 2011):

$$\Delta G(*H) = \Delta G(H^+ + e^-) \quad (3)$$

The term on the right, following the explanation before, has a value of 0 at E = 0 V (vs. NHE) and $-e_0E$ at a different potential E, where e_0 corresponds to the charge related to the number of electrons exchanged. This statement is correct assuming that when the potential changes, only the energy of the electrons is modified. DFT calculations are used to test this assumption, resulting in evidence that the binding energy of *H does not depend strongly on the potential, or on an applied electric field. For this reason, the standard equilibrium potential for the Volmer reaction is (Koper, 2011):

$$E^0{}_{H^+/*H} = -\frac{\Delta G^0(*H)}{e_0} \quad (4)$$

where $\Delta G^0(*\mathrm{H})$ is described as the adsorption energy of *H with reference to the energy of H_2. A thermodynamically favourable situation for the *H formation onto the catalyst surface, $E^0{}_{H^+/*H} > 0$, is obtained if $\Delta G^0(*\mathrm{H}) < 0$. Consequently, this situation for the overall reaction implies that (Koper, 2011):

$$E^0{}_{H^+/*H} = -E^0{}_{*H,H^+/H_2} \quad (5)$$

The standard equilibrium potential for the Heyrovsky reaction at these circumstances is below 0 V. This statement means that if the *H formation is thermodynamically favourable at E = 0 V, the Heyrovsky reaction has to be unfavourable as a negative equilibrium potential means that the reaction is not spontaneous, as ΔG would be positive: ΔG = -nFE for a reduction reaction (F is the Faraday constant and n the number of exchanged electrons). Then, the minimal thermodynamic overvoltage for the overall reaction, η_T, would be equal to the least favourable standard equilibrium potential in terms of thermodynamics. The overpotential is the potential difference (voltage) between a thermodynamically determined reduction potential and the potential at which the redox event is experimentally observed: $\eta_T = E^0{}_{H^+,*H/H_2} - E^0{}_{H^+/H_2}$. The thermodynamically least favourable step is called the potential-limiting step, which differs from the rate-determining step related to the highest activation energy that influences the kinetics of the reaction. In Figure 7 a two-step reaction is presented in which case (A) step 1 is rate determining and in (B) step 2 is rate determining. In both cases step 1 is the potential-limiting step, namely, step 1 determines the overpotential at which a certain current density may be reached.

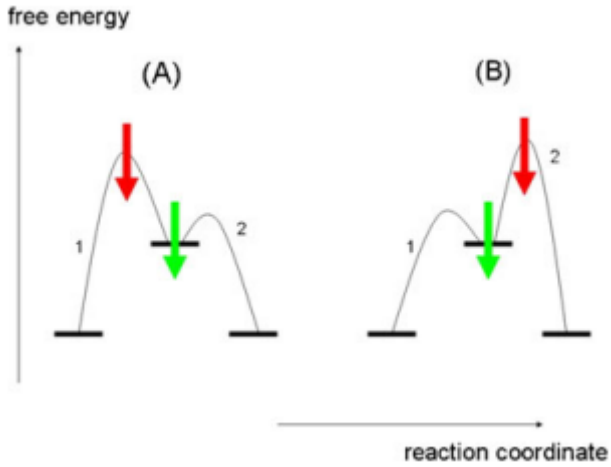

Figure 7. Two potential free energy landscapes for a two-step reaction. In A the potential-limiting step and the rate-determining step are the same (step 1), whereas in B they are different (1 and 2, respectively). Taken from (Koper, 2013).

We are looking for the lowest overpotential or driving force, which is zero for the HER, for this reason the catalyst must obey the next condition (Koper, 2011):

$$\eta_T = E^0{}_{H^+/*H} = E^0{}_{*H,H^+/H_2} = \frac{\Delta G^0(*H)}{e_0} = 0 \quad (6)$$

A catalyst with $\Delta G^0(*H) \neq 0$ results in a $\eta > 0$ because of a more negative than zero standard equilibrium potential from either the Volmer $\Delta G^0(*H) > 0$ or Heyrovsky $\Delta G^0(*H) < 0$ reactions. Figure 8 shows that the best catalyst is displays a tradeoff between strong and weak binding of the intermediate, *H. Such a graphic is called a Sabatier-type volcano plot. In this case, the descriptor used in the x-axis is the ability of the catalyst to bind *H.

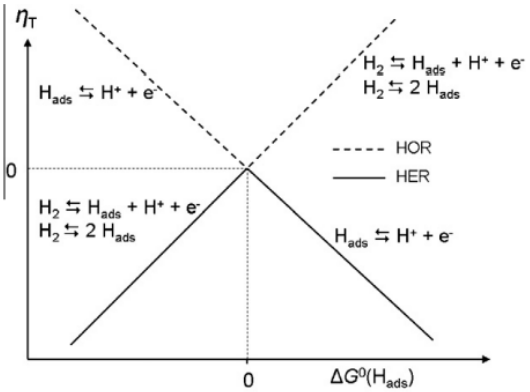

Figure 8. Volcano plot for the HER (solid lines) and HOR (dashed lines). The HER/HOR overpotentials are plotted as a function of free energy of adsorption of hydrogen on the electrode surface. Taken from (Koper, 2011).

The same analysis done previously for the Volmer/Heyrovsky mechanism can be applied to the Volmer/Tafel mechanism for the HER. The difference is that the Tafel reaction (1c) is not an electrochemical reaction so there is no standard equilibrium potential. Nonetheless, combined with reaction (1a), overall thermodynamic constraints must still be satisfied for reaction (1). The standard equilibrium constant of reaction (1c) is defined as (Koper, 2011):

$$K_{*H/H_2} = \exp\left[-\frac{\Delta G^0(*H)}{RT}\right] \quad (7)$$

The next relationship has to be followed for the Tafel/Volmer mechanism (Koper, 2011):

$$E^0{}_{H^+/*H} - \frac{\Delta G^0(*H)}{e_0} = 0 \quad (8)$$

If $E^0{}_{H^+/*H} < 0$, the thermodynamic overvoltage then is equal to this standard equilibrium potential. Conversely, if $E^0{}_{H^+/*H} > 0$, the Tafel reaction turns endothermic and consequently potential determining. Then, the thermodynamic overvoltage can be defined as $\eta_T = -E^0{}_{H^+/*H}$ from Equation 8.

3.4.2. How to go from EDFT to ΔG_H and η_{HER}

DFT calculations do not directly give free energies of adsorption to find out which surface has more activity towards the HER. Instead, we can use VASP to determine the energies of clean surfaces, surfaces with *H, and hydrogen gas to approximate the free energies of adsorption.

Free energies of adsorption, which correspond to the transition between the pure solid and the adsorbed phase energies, can be calculated using the next expression:

$$\Delta G = \Delta H - T\Delta S \quad (9)$$

Where ΔH is the enthalpy of adsorption and $T\Delta S$ is the product of the temperature times the entropy. The enthalpy of adsorption is the heat released or absorbed during the adsorption process and delta of entropy is a measurement of the change of disorder generated upon adsorption. The enthalpy can be approximated as the sum of two magnitudes, the DFT-calculated energy (E_{DFT}) and the zero-point energy (ZPE), that is the lowest possible energy that a quantum mechanical system may have (the term associated to a change of temperature is negligible to calculate the enthalpy of adsorption). For this reason, the Gibbs energy can be expressed as:

$$\Delta G = \Delta E_{DFT} + \Delta ZPE - T\Delta S \quad (10)$$

ΔE_{DFT} is calculated following Equation 11:

$$\Delta E_{DFT} = E_{*H} - \frac{1}{2}E_{H_2} - E_* \quad (11)$$

It is worth noting that half the energy of hydrogen ($1/2E_{H2}$) is used in Equation 11 to calculate the binding energy and not the energy of the proton (E_{H+}) and the electron (E_{e-}) involved in the process. The explanation to this is the equilibrium existent between the species ($1/2H_2 \leftrightarrows H^+ + e^-$).

To calculate the ΔZPE some simplifications are made. The change of zero-point energy of the surface with and without adsorbates is negligible. Thus, ΔZPE is approximated as:

$$\Delta ZPE \approx ZPE_{*H,fixed} - \frac{1}{2}ZPE_{H_2} \quad (12)$$

where $ZPE_{*H,fixed}$ is the zero-point energy of *H on a slab that is completely fixed at the coordinates found after the previous relaxation. Furthermore, the change of entropy can also be simplified. The entropy of the surface with and without *H are similar and negligible compared the entropy of hydrogen gas. This is justified knowing that the degree of disorder of gases is

considerably higher than solids, such that the entropy of hydrogen gas is the predominant term. The resulting expression to evaluate the variation of entropy is:

$$\Delta S \approx -\frac{1}{2}S_{H_2} \quad (13)$$

The free energy of adsorption incorporating all the previous considerations is given by Equation 14:

$$\Delta G = E_{*H} - \frac{1}{2}E_{H2} - E_{*} + ZPE_{*H} - \frac{1}{2}ZPE_{H2} + \frac{1}{2}TS_{H2} \quad (14)$$

All the energies presented in this work were calculated using DFT calculations except the entropy of H_2. Entropy in standard conditions can be determined from the nist thermodynamic tables (Hydrogen, n.d.). Also, temperature is considered 25 °C (298,15 K). The standard entropy of hydrogen is 130.68 J/mol·K.

Finally, once the Gibbs free adsorption energy (ΔG) has been calculated the thermodynamic minimum overvoltage (η_{HER}) can be obtained as: $\eta_{HER} = \frac{abs(\Delta G)}{e_0}$.

4. RESULTS AND DISCUSSION

At this point, the required theoretical background has been exposed and it is time to present the results obtained for the adsorption energies of *H on the (111) and (100) facets of Pt NSAs. Three important previous considerations are:

- The transition metals used in the simulations in the subsurface layers are: Scandium (Sc), Titanium (Ti), Vanadium (V), Chromium (Cr), Manganese (Mn), Iron (Fe), Cobalt (Co), Nickel (Ni), Copper (Cu), Zinc (Zn), Yttrium (Y), Zirconium (Zr), Niobium (Nb), Molybdenum (Mo), Technetium (Tc), Ruthenium (Ru), Rhodium (Rh), Palladium (Pd), Silver (Ag), Cadmium (Cd), Lanthanum (La), Hafnium (Hf), Tantalum (Ta), Tungsten (W), Rhenium (Re), Osmium (Os), Iridium (Ir), Platinum (Pt), Gold (Au) and Mercury (Hg).
- Energies are obtained for the various possible adsorption sites on the (111) and (100) facets. For (111) facets the possible adsorption sites are top, bridge, HCP hollow, FCC hollow. On the other hand, for (100) facets, the possible sites are top, bridge and HCP hollow. Figure 2 displays the possible adsorptions sites on (111) and (100).
- All numerical results are provided in the appendices of this work for both (111) and (100) facets of Pt NSAs.

4.1. ADSORPTION ENERGIES OF *H ON THE (111) AND (100) FACETS OF PT NSAS

First, the **results for (111) facets of Pt NSAs** are presented and discussed in detail.

In order to obtain binding energies, which are expressed in eV, all input files that VASP needs have to be correctly elaborated for all clean surfaces and surfaces with *H. Also, input files have to be adapted to calculate the energy of the hydrogen gas molecule. The Visual Molecular Dynamics (VMD) software was used to obtain the correct Cartesian coordinates of the various possible adsorption sites, necessary to elaborate all POSCAR files for surfaces with *H. The metal slabs were taken from previous works (Tymoczko et al., 2016) (Pohl et al., 2017). This is possible because VMD allows the free movement of atoms and shows the final coordinates. The Cartesian

coordinates obtained and the distances in Angstrom between hydrogen and platinum atom(s) on (111) facets of Pt NSAs are in Table A1.1 of the appendix section.

After creating all the necessary input files for all the systems (seen in Background and more precisely VASP section of the research), DFT energies are calculated for each NSA surface with and without adsorbed hydrogen and for the hydrogen gas molecule. The DFT total energy for the hydrogen gas molecule is calculated only once and has a value of -6.77 eV using PBE and the PAW method.

There were cases in which the required accuracy was not reached and the results were not meaningful. The situations in which this problem occurred, all involving surfaces with *H, and the way they were solved are:

- Sc top, bridge, HCP hollow and FCC hollow: the calculations were made again.
- Y HCP hollow: The convergence criteria for the forces was relaxed from 0.01 to 0.025 eV/Å.
- Re bridge and HCP hollow: The convergence criteria for the forces was relaxed from 0.01 to 0.025 eV/Å.
- La top, bridge, HCP hollow and FCC hollow: First the convergence criteria was relaxed and then, as no valid result was obtained, the ion relaxation was allowed for the adsorbate while the surface was fixed, by the setting the degrees of freedom of the POSCAR to F F F for all surface atoms.

Then, the most stable DFT energy of the surface with *H was selected among all the possible adsorption sites and was used to determine the adsorption energy (ΔE_{DFT}), together with the matching clean surface energy and the energy of hydrogen molecule, using Equation 11. VMD was used to corroborate that ion relaxation has not moved the adsorbate to a different adsorption site, using the CONTCAR of the most stable site. The corroboration performed at the most stable sites showed that all bridge adsorbates on (111) terraces moved to FCC sites.

In order to determine whether the results are accurate an analysis of them is carried out. In Figure 9 we plot the adsorption energy of hydrogen as a function of the number of valence electrons of the subsurface metals (denoted as N). Since we simulated NSAs with 3d, 4d and 5d metals, for a given number of electrons there are three alloys. For instance, for N = 8, the three NSAs are Pt-Fe, Pt-Ru and Pt-Os. The number of valence electrons of each transition metal studied are in Table 1.

Table 1. Number of valence electrons of the d-block elements studied and total number of valence electrons in the Pt-X NSAs (Pt + H + Xi). Xi is the transition metal.

Number of valence electrons	Number of total valence electrons	d-block elements (transition metals)		
		3d	4d	5d
3	14	Sc	Y	La
4	15	Ti	Zr	Hf
5	16	V	Nb	Ta
6	17	Cr	Mo	W
7	18	Mn	Tc	Re
8	19	Fe	Ru	Os
9	20	Co	Rh	Ir
10	21	Ni	Pd	Pt
11	22	Cu	Ag	Au
12	23	Zn	Cd	Hg

As mentioned before, differences in valence configurations have a direct impact on adsorption energies, but one can expect that alloys with a given N will behave similarly. Therefore, the three d series of transition metals should display similar tendencies as a function of N and the differences between series should be small. Accordingly, if for a given N there is a datapoint that does not follow the trends of the other two, that alloy is to be analysed in detail. When the trends have clear outliers, there are two options:

1. Recalculate the energy of the clean surface using the CONTCAR of the surface with *H as the new POSCAR (removing *H from it), to evaluate the new clean surface. This is useful when there are small surface reconstructions upon *H adsorption.
2. If the first option does not work, fix all positions of the metal slab except the adsorbate and recalculate. This is useful when there are large surface reconstructions.

On the (111) terrace Y, Cr and Mn did not follow the overall trends, so correction 1 was applied to Y, while correction 2 was applied to Cr and Mn. Figure 9 incorporates all the corrected values.

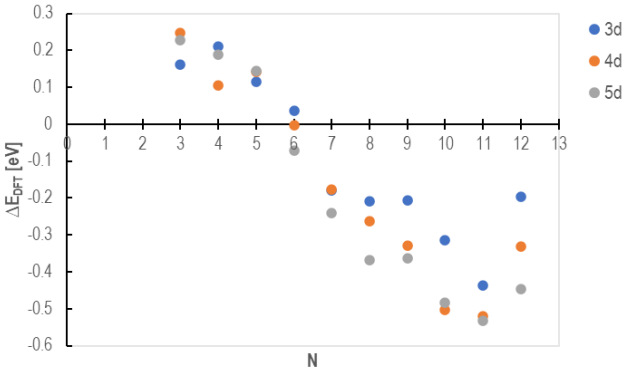

Figure 9. DFT energies of adsorption of hydrogen as a function of the number of valence electrons of the subsurface metals for (111) Pt NSAs.

Figure 9 shows that the alloys for which the adsorption energy is minimal have N = 11. Previous works have shown that (1) adsorption energies are a function of both the number of valence electrons of the surface components and that of the adsorbate and (2) the most stable adsorption energies are expected when the electron cloud surrounding an atom resembles that of a noble gas (the octet rule for light elements and the 18-electron rule for heavy elements), which for (111) NSAs happens at a total number of valence electrons of 24 (Calle-Vallejo et al., 2012).

The total number of valence electrons at the minimum adsorption energy is 22 valence electrons in Figure 9, since the minima are on N = 11, Pt has 10 valence electrons and H has 1. The different minima (24 vs 22) are justified because in the previous work only adsorption atop was considered, while here the adsorption site giving the most negative DFT energy was selected to calculate the adsorption energy. Figure 10 provides a comparison of the adsorption energies between top sites and the most stable site for 3d NSAs. Noticeably, *H on top sites using a 3d transition metal has a minimum of adsorption energy at 7 to 8 valence electrons, such that the minimum is at N = 7, which corresponds to a Pt-Mn NSA. In such an alloy, Pt and Mn fulfil the 18-electron rule and the 1s orbital of H is full.

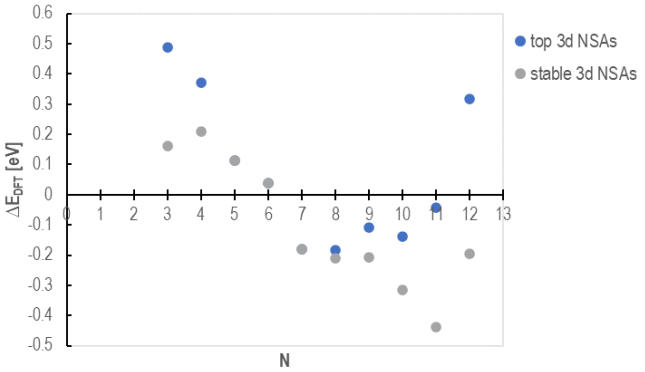

Figure 10. Differences in adsorption energies between top sites and the most stable sites for Pt(111) NSAs with 3d metals.

Furthermore, the ZPE values were gathered and analysed using VASP. The particularities of these calculations are that (1) the CONTCAR obtained from the initial DFT optimization is the new POSCAR, and (2) the INCAR file has to be adjusted so that the algorithms and the parameters that VASP needs to evaluate the vibrational frequencies are correctly set. The INCAR tags to determine the vibrational frequencies are in the Background section, more precisely in the subsection devoted to VASP.

After creating all the essential inputs, the vibrational frequencies are calculated for every surface with *H and for hydrogen in the gas phase. The ZPE for the hydrogen gas molecule is 0.28 eV. As explained before, the frequencies of the clean surfaces do not have to be evaluated. In the end: $ZPE = 1/2 \sum \hbar v_i$, where v_i are the DFT-calculated frequencies and $\hbar$ is the reduced Planck constant. Figure 11 shows the change of the zero-point energy of adsorption calculated with Equation 12 as a function of the number of valence electrons. We observe in Figure 11 that DZPE is in no case larger than 0.05 eV.

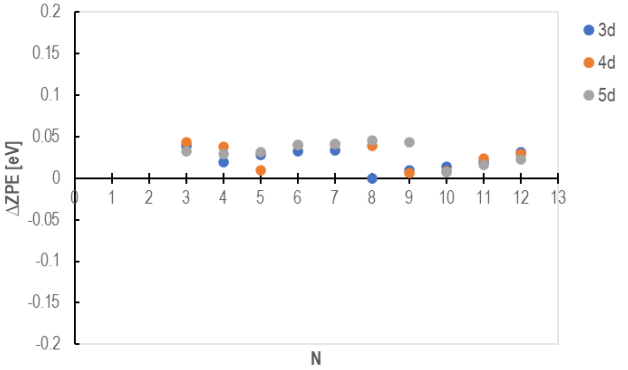

Figure 11. Zero-point energies of adsorption faced with the number of valence electrons for (111) facets of Pt NSAs.

Finally, the only term missing to approximate the free energies of adsorption is the entropy correction. Adsorption entropy is evaluated using equation 13. The standard entropy of hydrogen gas molecule is 0.00135 eV/K, such that $T\Delta S = 0.404$ eV, considering T = 298.15 K. Then, Gibbs free adsorption energies are determined using equation 14. Figure 12 shows the free energies of adsorption as a function of the number of valence electrons.

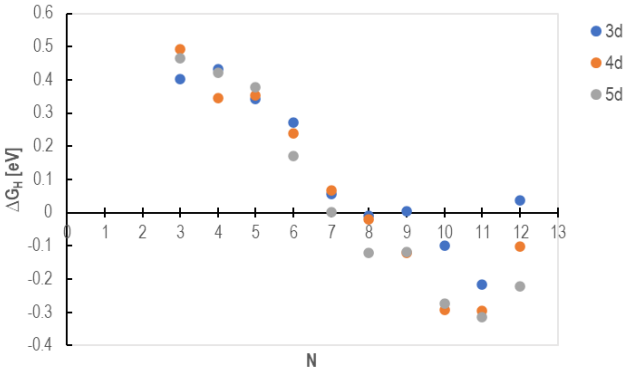

Figure 12. Free energies of adsorption of hydrogen as a function of the number of valence electrons of the alloying metal for the (111) facet of Pt NSAs.

The trends are analogous to those of Figure 9, as ΔE_{DFT} is the predominant term to determine the free energies of adsorption, the entropy corrections are identical for all alloys and the changes in ZPE in Figure 11 are rather small. Again, the number of valence electrons with the lowest free energies of adsorption energy is found at N = 11.

In the following, the **results for (100) facets of Pt NSAs** are presented and discussed in detail. The method for assessing the free energies is the same followed for (111) facets. The only change is the use of a POSCAR file with the (100) coordinates and lattice vectors for all the present systems, while all other files remain the same. Note that (100) terraces have three possible adsorption sites (top, bridge and HCP hollow), as seen in Figure 2b. The Cartesian coordinates obtained and the distances in Angstrom between hydrogen and platinum atom(s) on (100) facets of Pt NSAs are in Table A2.1 of Appendix 2.

First, Figure 13 presents all binding energies determined. As before for (111) facets, there were cases in which the required accuracy was not reached. The cases in which this occurred and how it was overcome were:

- Ti HCP hollow: The calculations were remade.
- Pd HCP hollow: The calculations were remade.
- Pt HCP hollow: The convergence criteria was relaxed.

- Hg HCP hollow: The convergence criteria was relaxed.

Hydrogen adsorption on HCP hollow site is more problematic for (100) terraces than bridge and top sites during ion relaxation as no problem with accuracy was observed for the latter two adsorption sites. In almost all systems hydrogen adsorption on bridge sites is preferred, apart from few cases in which the intermediate prefers HCP hollows.

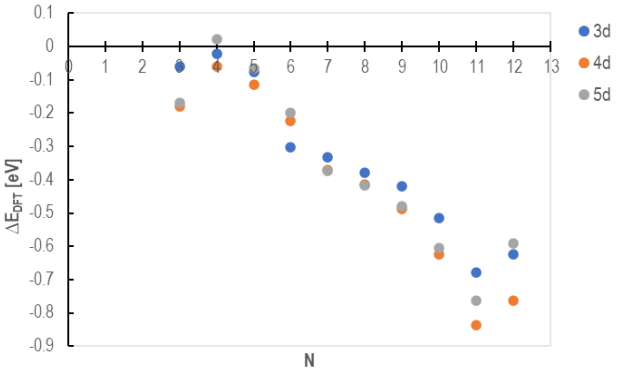

Figure 13. DFT-calculated energies of adsorption of hydrogen as a function of the number of valence electrons of the alloying metal for the (100) facet of Pt NSAs.

The analysis for detecting outliers in the binding energy trends is done using Figure 13. The (100) facet of La, Mn, Ag and Hg NSAs did not follow the trends and so all displacements were corrected by recalculating the energy of the clean surface with the CONTCAR file of the slab with *H.

The binding energy is minimal at N = 22, as on (111) terraces. The adsorption energies are more negative, namely, more stable, on the (100) terrace compared to the (111) terrace. The changes in zero-point energy obtained are provided in Figure 14. As observed for the (111) facets, DZPE is small for all NSAs.

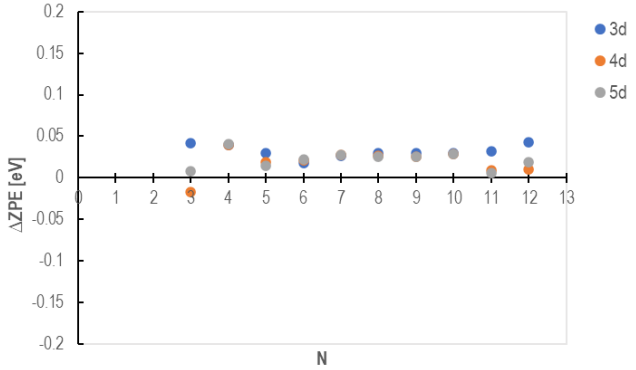

Figure 14. Zero-point energies of adsorption faced with the number of valence electrons for (100) facets of Pt NSAs.

Finally, the only contribution missing is from entropy and, because of the simplifications applied, it is the same as for the (111) NSAs. The final free adsorption energies are displayed in Figure 15. The resulting free energies of adsorption obtained for (100) terraces are more negative than for (111) terraces but the trends are similar.

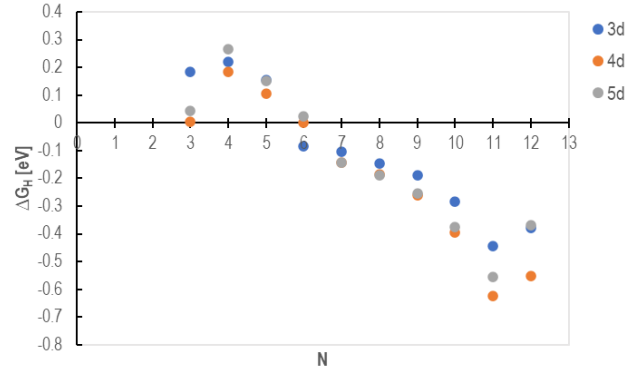

Figure 15. Free adsorption energies as a function of the number of valence electrons for the (100) facet of Pt NSAs.

4.2. **VOLCANO PLOTS AND ACTIVE CANDIDATES**

First, the **results for (111) facets of Pt NSAs** are presented and discussed in detail.

After obtaining all the free adsorption energies for all the different electrodes the minimum overpotential required is evaluated using Equation 6. Figure 16 exhibits the additive inverse minimum HER overpotentials versus the number of valence electrons.

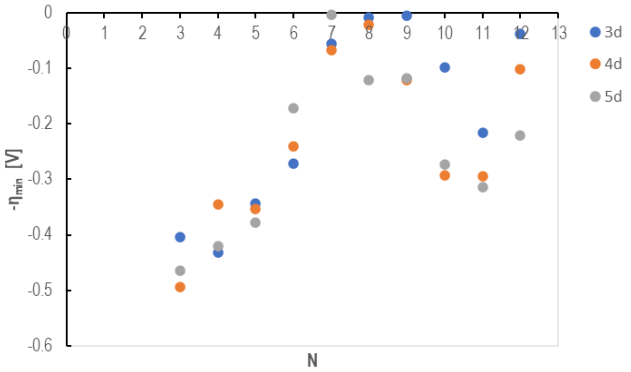

Figure 16. Additive inverse of the minimum HER overpotentials plotted against the number of valence electrons of the alloying metal for (111) facets of Pt NSAs.

To have a clearer appreciation of how the number of valence electrons influences the minimum HER overpotential, the average of the minimum overpotentials was calculated for each number of valence electrons together with their respective standard deviation. Figure 17 shows the additive inverse of the average minimum overpotentials as a function of the number of valence electrons. The overpotential closest to 0 V, which is the overpotential of interest, is located at 7-9 valence electrons. These range of electrons (together with N = 12) guarantee that, in line with the Sabatier principle, *H binding is neither too weak nor too strong.

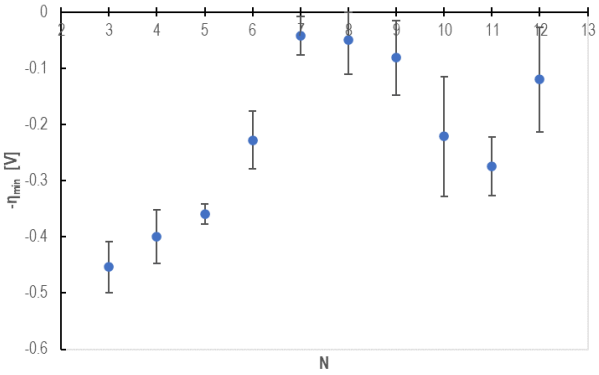

Figure 17. Additive inverse of the average minimum HER overpotentials versus the number of valence electrons of alloying metal for the (111) facets of Pt NSAs. The error bars correspond to the standard deviation of the three alloys with the same N.

Figure 18 presents the volcano plot of HER activity for the (111) facet of Pt NSAs. The left part of the plot ($\Delta G < 0$) is occupied by strong-binding alloys for which H_2 desorption is problematic. On the other hand, the right part ($\Delta G > 0$) is occupied by weak-binding alloys in which *H adsorption is problematic.

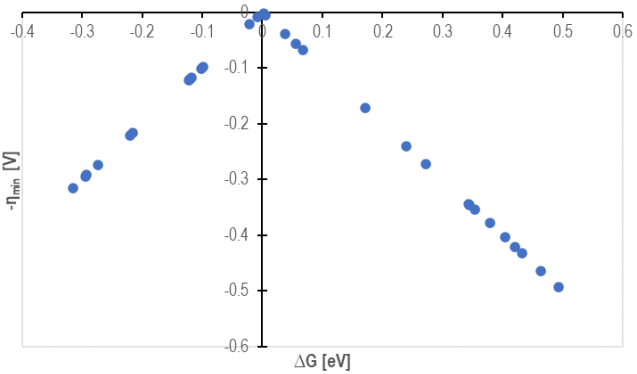

Figure 18. Volcano plot correlating the additive inverse of the HER overpotential and the free energy of adsorption of hydrogen for the (111) facet of Pt NSAs.

The most active candidates on the (111) facet of Pt NSAs are selected stablishing an overpotential limit of no more than 0.1 V. The active candidates that meet this requirement contain the following d metals: Mn, Fe, Co, Ni, Zn, Tc, Ru and Re.

Figures 19, 20 and 21 show the **results for (100) facets of Pt NSAs**. The number of electrons that guarantee that, in line with the Sabatier principle, *H binding is neither too weak nor too strong are N = 3 and N = 6. The active candidates that meet the requirement stablished previously (minimum overpotential of less than 0.1 V) are: Cr, Y, Mo, La, W.

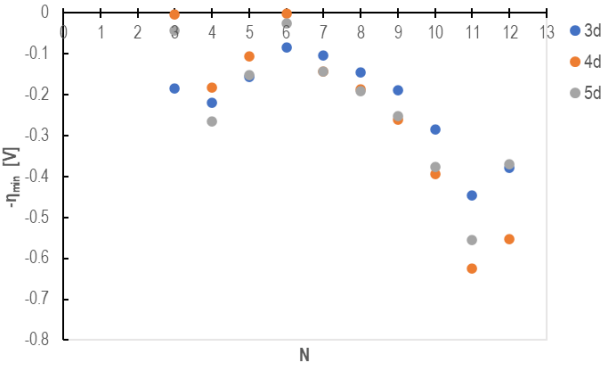

Figure 19. Additive inverse of the minimum overpotential as a function of the number of valence electrons of the alloying metal for the (100) facet of Pt NSAs.

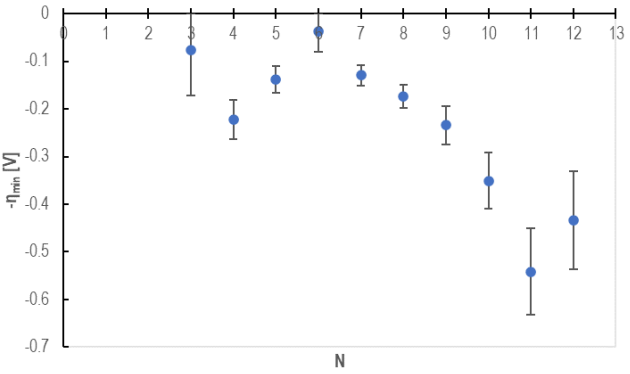

Figure 20. Additive inverse of the average minimum overpotentials faced with the number of valence electrons for (100) facets of Pt NSAs. The error bars correspond to the standard deviation of the three alloys with the same N.

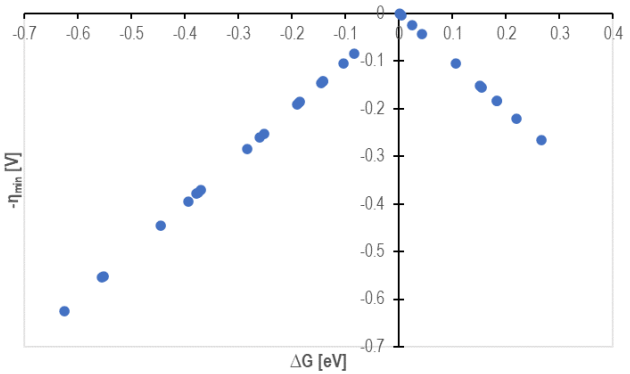

Figure 21. Volcano plot for the HER catalysed by the (100) facet of Pt NSAs.

Figure 22 provides a clearer view of the HER trends for the two facets studied. It displays the additive inverse of the average minimum overpotentials as a function of the number of valence electrons for the (100) and (111) facets of Pt NSAs. We observe that number of electrons with the most active NSAs, for both facets are 7,8,9 and 12 electrons for (111), and for the (100) NSAs 6 and 3 electrons are most active. The difference might be caused by (a) the different coordination number of the two facets, given that for the (111) facet the coordination number is 9 and for the (100) facet it is 8, and (b) the fact that the most common adsorption sites are different for the two facets: hollows on the (111) and bridge sites on the (100).

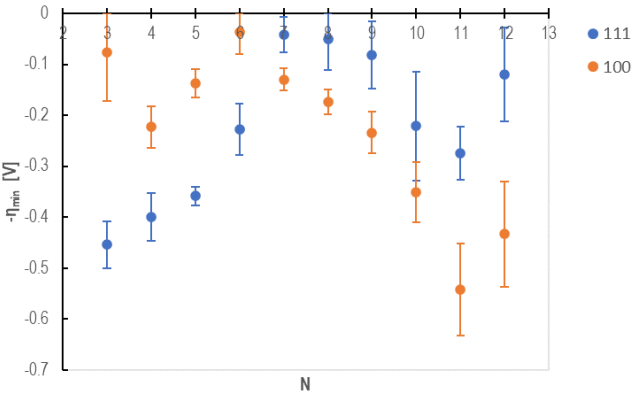

Figure 22. Additive inverse of the average minimum overpotentials faced with the number of valence electrons for (100) facets of Pt NSAs and (111) facets of Pt NSAs. The error bars correspond to the standard deviation of the three alloys with the same N and facet.

CONCLUSIONS

From the results obtained in this work the following conclusions can be drawn:

- The hydrogen binding energy is a good descriptor for optimizing HER catalysts.
- The optimal HER catalytic surface should bind *H with $\Delta G_H \approx 0$, resulting in a minimum overpotential close to 0.
- VASP, a code based on density functional theory, is an efficient tool to determine free energies of adsorption.
- The most active candidates on the (111) facet of Pt NSAs have the following transition metals in the subsurface: Mn, Fe, Co, Ni, Zn, Tc, Ru, Re.
- The most active candidates for (100) facets of Pt NSAs are Cr, Y, Mo, La, W.
- The number of electrons with the most active NSAs is 7 electrons for (111) facets and 6 electrons for (100) facets. The difference might be caused by the different coordination number of the two facets (9 for the (111) and 8 for the (100)).

APPENDICES

APPENDIX 1: DATA FOR THE (111) FACET OF PT NSAS

Table A1.1. Cartesian coordinates of the initial guesses for the *H adsorbates on the (111) facets of Pt NSAs, and distances between the adsorbate and the platinum atom(s).

Adsorption Site	**Cartesian coordinates** [Å]			**Distance** [Å]
Top	0.014	0.009	1.811	1.81
Bridge	0.660	1.237	1.122	1.80 and 1.80
HCP	1.393	0.806	1.124	1.98, 1.98 and 1.96
FCC	2.815	1.652	1.120	1.96, 1.96 and 2.00

Table A1.2. DFT binding energies evaluated with *H on the most stable adsorption site (ΔE) and on top (ΔEtop).

Pt alloys	ΔE_{top} [eV]	ΔE [eV]	Pt alloys	ΔE_{top} [eV]	ΔE [eV]
Sc	0.49	0.16	**Ru**	-0.26	-0.26
Ti	0.37	0.21	**Rh**	-0.27	-0.33
V	0.11	0.11	**Pd**	-0.37	-0.50
Cr	0.04	0.04	**Ag**	-0.13	-0.52
Mn	-0.18	-0.18	**Cd**	0.06	-0.33
Fe	-0.18	-0.21	**La**	0.83	0.23
Co	-0.11	-0.21	**Hf**	0.57	0.19
Ni	-0.14	-0.31	**Ta**	0.15	0.15
Cu	-0.04	-0.44	**W**	-0.07	-0.07
Zn	0.32	-0.20	**Re**	-0.24	-0.24
Y	0.80	0.25	**Os**	-0.37	-0.37
Zr	0.61	0.11	**Ir**	-0.36	-0.36
Nb	0.23	0.14	**Pt**	-0.44	-0.48
Mo	0.00	0.00	**Au**	-0.31	-0.53
Tc	-0.18	-0.18	**Hg**	-0.18	-0.45

Table A1.3. Most stable adsorption site for *H.

alloying metal	site	alloying metal	site
Sc	HCP	**Ru**	top
Ti	HCP	**Rh**	FCC
V	top	**Pd**	FCC
Cr	top	**Ag**	FCC
Mn	top	**Cd**	FCC
Fe	FCC	**La**	HCP
Co	FCC	**Hf**	HCP
Ni	FCC	**Ta**	top
Cu	FCC	**W**	top
Zn	FCC	**Re**	top
Y	HCP	**Os**	top
Zr	HCP	**Ir**	top
Nb	FCC	**Pt**	FCC
Mo	top	**Au**	FCC
Tc	top	**Hg**	FCC

Table A1.4. ZPE values for surfaces with *H and DZPE of adsorption.

alloying metal	ZPE_{*H} [eV]	ΔZPE [eV]	alloying metal	ZPE_{*H} [eV]	ΔZPE [eV]
Sc	0.18	0.04	**Ru**	0.18	0.04
Ti	0.16	0.02	**Rh**	0.15	0.01
V	0.17	0.03	**Pd**	0.15	0.01
Cr	0.17	0.03	**Ag**	0.16	0.02
Mn	0.17	0.03	**Cd**	0.17	0.03
Fe	0.14	0.00	**La**	0.17	0.03
Co	0.15	0.01	**Hf**	0.17	0.03
Ni	0.15	0.01	**Ta**	0.17	0.03
Cu	0.16	0.02	**W**	0.18	0.04
Zn	0.17	0.03	**Re**	0.18	0.04
Y	0.18	0.04	**Os**	0.19	0.05
Zr	0.18	0.04	**Ir**	0.18	0.04
Nb	0.15	0.01	**Pt**	0.15	0.01
Mo	0.18	0.04	**Au**	0.16	0.02
Tc	0.18	0.04	**Hg**	0.16	0.02

Table A1.5. Free energies of adsorption and additive inverse of the minimum overpotentials.

alloying metal	ΔG [eV]	$-\eta_{min}$ [V]	alloying metal	ΔG [eV]	$-\eta_{min}$ [V]
Sc	0.40	-0.40	**Ru**	-0.02	-0.02
Ti	0.43	-0.43	**Rh**	-0.12	-0.12
V	0.34	-0.34	**Pd**	-0.29	-0.29
Cr	0.27	-0.27	**Ag**	-0.29	-0.29
Mn	0.06	-0.06	**Cd**	-0.10	-0.10
Fe	-0.01	-0.01	**La**	0.46	-0.46
Co	0.01	-0.01	**Hf**	0.42	-0.42
Ni	-0.10	-0.10	**Ta**	0.38	-0.38
Cu	-0.22	-0.22	**W**	0.17	-0.17
Zn	0.04	-0.04	**Re**	0.00	0.00
Y	0.49	-0.49	**Os**	-0.12	-0.12
Zr	0.35	-0.35	**Ir**	-0.12	-0.12
Nb	0.35	-0.35	**Pt**	-0.27	-0.27
Mo	0.24	-0.24	**Au**	-0.31	-0.31
Tc	0.07	-0.07	**Hg**	-0.22	-0.22

Table A1.6. Additive inverse of the average minimum overpotential together with its respective standard deviation for every number of valence electrons.

N	Average $-\eta_{min}$ [V]	Standard deviation [V]
3	-0.45	0.05
4	-0.40	0.05
5	-0.36	0.02
6	-0.23	0.05
7	-0.04	0.03
8	-0.05	0.06
9	-0.08	0.07
10	-0.2	0.1
11	-0.27	0.05
12	-0.12	0.09

APPENDIX 2: DATA FOR THE (100) FACET OF PT NSAS

Table A2.1. Cartesian coordinates of the initial guesses for the *H adsorbates on (100) facets of Pt NSAs, and distances between the adsorbate and the platinum atom(s).

Adsorption Site	**Cartesian coordinates [Å]**	**Distance** [Å]
Top	0.014 0.009 1.811	1.81
Bridge	0.001 1.398 1.143	1.81 and 1.82
HCP	1.387 1.387 1.146	2.27 2.30 2.30 and 2.32

Table A2.2. DFT binding energies of *H on the most stable adsorption site (ΔE).

alloying metals	ΔE [eV]	alloying metals	ΔE [eV]
Sc	-0.06	**Tc**	-0.37
Ti	-0.02	**Ru**	-0.41
V	-0.08	**Rh**	-0.49
Cr	-0.30	**Pd**	-0.62
Mn	-0.33	**Ag**	-0.84
Fe	-0.38	**Cd**	-0.76
Co	-0.42	**La**	-0.17
Ni	-0.52	**Hf**	0.02
Cu	-0.68	**Ta**	-0.06
Zn	-0.62	**W**	-0.20
Y	-0.18	**Re**	-0.37
Zr	-0.06	**Os**	-0.42
Nb	-0.11	**Ir**	-0.48
Mo	-0.22	**Pt**	-0.61
Tc	-0.37	**Au**	-0.76
Ru	-0.41	**Hg**	-0.59

Table A2.3. Most stable site for every surface with *H.

alloying metal	site	alloying metal	site
Sc	bridge	**Ru**	bridge
Ti	bridge	**Rh**	bridge
V	bridge	**Pd**	bridge
Cr	bridge	**Ag**	HCP
Mn	bridge	**Cd**	HCP
Fe	bridge	**La**	HCP
Co	bridge	**Hf**	bridge
Ni	bridge	**Ta**	bridge
Cu	bridge	**W**	bridge
Zn	bridge	**Re**	bridge
Y	HCP	**Os**	bridge
Zr	bridge	**Ir**	bridge
Nb	bridge	**Pt**	bridge
Mo	bridge	**Au**	HCP
Tc	bridge	**Hg**	HCP

Table A2.4. ZPE values for surfaces with *H and ZPE of adsorption.

alloying metal	ZPE_{*H} [eV]	ΔZPE [eV]	alloying metal	ZPE_{*H} [eV]	ΔZPE [eV]
Sc	0.18	0.04	**Ru**	0.17	0.03
Ti	0.18	0.04	**Rh**	0.17	0.03
V	0.17	0.03	**Pd**	0.17	0.03
Cr	0.16	0.02	**Ag**	0.15	0.01
Mn	0.17	0.03	**Cd**	0.15	0.01
Fe	0.17	0.03	**La**	0.15	0.01
Co	0.17	0.03	**Hf**	0.18	0.04
Ni	0.17	0.03	**Ta**	0.15	0.01
Cu	0.17	0.03	**W**	0.16	0.02
Zn	0.18	0.04	**Re**	0.17	0.03
Y	0.12	-0.02	**Os**	0.17	0.03
Zr	0.18	0.04	**Ir**	0.16	0.02
Nb	0.16	0.02	**Pt**	0.17	0.03
Mo	0.16	0.02	**Au**	0.15	0.01
Tc	0.17	0.03	**Hg**	0.16	0.02

Table A2.5. Free energies of adsorption and additive inverse of the minimum overpotentials.

alloying metal	ΔG [eV]	$-\eta_{min}$ [V]	alloying metal	ΔG [eV]	$-\eta_{min}$ [V]
Sc	0.18	-0.18	**Ru**	-0.19	-0.19
Ti	0.22	-0.22	**Rh**	-0.26	-0.26
V	0.16	-0.16	**Pd**	-0.39	-0.39
Cr	-0.08	-0.08	**Ag**	-0.63	-0.63
Mn	-0.10	-0.10	**Cd**	-0.55	-0.55
Fe	-0.15	-0.15	**La**	0.04	-0.04
Co	-0.19	-0.19	**Hf**	0.27	-0.27
Ni	-0.28	-0.28	**Ta**	0.15	-0.15
Cu	-0.45	-0.45	**W**	0.02	-0.02
Zn	-0.38	-0.38	**Re**	-0.14	-0.14
Y	0.00	0.00	**Os**	-0.19	-0.19
Zr	0.18	-0.18	**Ir**	-0.25	-0.25
Nb	0.11	-0.11	**Pt**	-0.38	-0.38
Mo	0.00	0.00	**Au**	-0.55	-0.55
Tc	-0.14	-0.14	**Hg**	-0.37	-0.37

Table A2.6. Additive inverse of the average minimum overpotential together with its respective standard deviation, for every number of valence electrons.

N	Average $-\eta_{min}$ [V]	Standard deviation [V]
3	-0.08	0.09
4	-0.22	0.04
5	-0.14	0.03
6	-0.04	0.04
7	-0.13	0.02
8	-0.17	0.02
9	-0.23	0.04
10	-0.35	0.06
11	-0.54	0.09
12	-0.4	0.1